Materials and Design 32 (2011) 4509–4520

Contents lists available at ScienceDirect

Materials and Design

journal homepage: www.elsevier.com/locate/matdes

Fatigue crack growth behaviour of gas tungsten arc, electron beam and laser beam welded Ti–6Al–4V alloy

T.S. Balasubramanian [a], V. Balasubramanian [b,*], M.A. Muthu Manickam [a]

[a] Combat Vehicle Research and Development Establishment (CVRDE), Avadi, Chennai 600 054, India
[b] Center for Materials Joining & Research (CEMAJOR), Department of Manufacturing Engineering, Annamalai University, Annamalainagar 608 002, Tamil Nadu, India

ARTICLE INFO

Article history:
Received 3 October 2010
Accepted 14 March 2011
Available online 21 March 2011

Keywords:
A. Non ferrous metals and alloys
D. Welding
E. Fatigue

ABSTRACT

The present investigation is aimed to evaluate fatigue crack growth parameters of gas tungsten arc, electron beam and laser beam welded Ti–6Al–4V titanium alloy for assessing the remaining service lives of existing structure by fracture mechanics approach. Center cracked tensile specimens were tested using a 100 kN servo hydraulic controlled fatigue testing machine under constant amplitude uniaxial tensile load. Crack growth curves were plotted and crack growth parameters (exponent and intercept) were evaluated. Fatigue crack growth behavior of welds was correlated with mechanical properties and microstructural characteristics of welds. Of the three joints, the joint fabricated by laser beam welding exhibited higher fatigue crack growth resistance due to the presence of fine lamellar microstructure in the weld metal.

1. Introduction

Ti–6Al–4V alloy has important characteristics such as high strength to weight ratio, excellent corrosion resistance, good toughness, low thermal expansion rate, high temperature creep resistance and good formability. The welds and welded joints of Ti–6Al–4V alloy fabricated in nuclear engineering, civil industries, transportable bridge girders, military vehicles, road tankers and space vehicles [1–3] are subjected to fluctuating loads. This kind of loading causes small cracks to grow during life of the component and leads to fatigue failure. A detailed study of this crack growth measurement could prevent the failure with prediction, which could ensure that the crack will never propagate and fail prior to detection. This necessitates a fatigue crack growth measurement of the Ti–6Al–4V alloy welded joints to avoid catastrophic failure.

The welding technology of titanium is complicated due to the fact that at temperatures above 550 °C, and particularly in the molten stage, it is known to be very reactive towards atmospheric gases such as oxygen, nitrogen, carbon or hydrogen causing severe embrittlement [4]. Gas tungsten arc welding (GTAW) is a most preferred welding method for reactive materials like titanium alloy due to its comparatively easier applicability and better economy [5]. Laser beam welding (LBW) process is used for welding of titanium alloys due to its advantages such as precision and noncontact processing, with a small heat affected zone (HAZ), consistent and reliable joints, etc. [4]. Electron beam welding (EBW) is highly suitable for joining of titanium, due to high vacuum inside the chamber where the process is carried out, which shields hot metal from contamination [2].

Fatigue crack growth behavior of α + β Ti–Al–Mn alloy welded by an automated GTAW, manual GTAW and EBW processes was investigated by Keshava Murthy and Sundaresan [6]. They reported that a significant increase in fatigue crack growth resistance was due to the presence of tensile residual stress normal to the fatigue load in addition with lamellar microstructure. Saxena and Radhakrishnan [7] variegated the effect of phase morphology of fatigue crack growth behavior of α + β titanium alloy and reported that the fatigue crack growth was strongly influenced by the phase morphology. A study was carried out by Sinha et al. [8] variegated the effects of positive stress ratios on the propagation of long and short fatigue cracks in mill annealed Ti–6Al–4V alloy. They opined that the effects of stress ratio on fatigue crack growth rates can also be rationalized largely by crack closure arguments. Differences between the long and the short crack behaviour at low stress ratios are attributed to lower levels of crack closure in the short crack regime. Boyce and Ritchie [9] investigated that the influence of load ratio and maximum stress intensity and found that crack growth and threshold are independent of loading frequency up to 50–1000 Hz. The fatigue thresholds were found to vary significantly with positive load ratio ($R = 0.1–0.95$). At load ratios larger than 0.5–0.95, where (global) crack closure could no longer be detected.

Tsay et al. [10] explored the influence of porosity on the fatigue crack growth behavior of Ti–6Al–4V alloy laser welds and concluded that the effect of porosity against fatigue crack growth

* Corresponding author. Tel.: +91 4144 239734 (O), +91 4144 241147 (R), mobile: +91 9443412249; fax: +91 4144 238080/238275.
E-mail addresses: tsbraja@yahoo.com (T.S. Balasubramanian), balasubramanian.v.2784@annamalaiuniversity.ac.in, visvabalu@yahoo.com (V. Balasubramanian), mamuthumanickam@yahoo.com (M.A. Muthu Manickam).

0261-3069/$ - see front matter © 2011 Elsevier Ltd. All rights reserved.
doi:10.1016/j.matdes.2011.03.025

resistance was less at lower stress ratio compared to higher stress ratio. Ding et al. [11] studied the effect of hydrogen on fatigue crack growth behaviour of Ti–6Al–4V and reported that hydrogen embrittlement enhanced cracking and alleviated the effect of crack deflections in Ti–6Al–4V at a higher stress ratio of 0.5. Wang et al. [12] analyzed the influences of precrack orientations in welded joint of Ti–6Al–4V on fatigue crack growth. It was also reported that the specimen with precrack along the weld center line exhibited lower fatigue crack propagation rate and significantly higher threshold stress intensity than the base metal specimen. Although crack path fluctuations and crack bifurcations occurred frequently in martensite structures of fusion zone (FZ), in the initial propagation stage, the crack in the specimen with precrack along the weld center line propagated by striation mechanism, not cleavage mechanism.

Though recent improvements in welding techniques that allow to realize high quality welded joints, the joint properties are greatly influenced by the welding processes. Apart from the basic design of the new structure, there is also increasing interest in methods for assessing the remaining service lives of existing structure by the fracture mechanics approach, where fatigue crack growth data are used in conjunction with the stress intensity factor to calculate the progress of a known flaw. From the literature review, it is understood that the extensive research work has been carried out on fatigue behaviour of forgings and bars of Ti–6Al–4V alloy. Most of the published information focuses on the effect of stress ratio, surface characteristics, phase morphology and residual stress on crack growth behaviour. However, there is no literature available comparing the fatigue crack growth resistance of GTAW, LBW and EBW joints of rolled plates of Ti–6Al–4V alloy. Hence, the present investigation was carried out to understand the fatigue crack growth behaviour of GTAW, LBW and EBW joints of Ti–6Al–4V alloy.

2. Experimental work

The rolled plates of 5.4 mm thick Ti–6Al–4V alloy were used to fabricate the joints. The chemical composition of the base metal is presented in Table 1. The optical micrograph of base metal is shown in Fig. 1. It contains bimodal structure of elongated grains of 'α' (light etched) and transformed 'β' (dark etched) in addition with some amount of acicular 'α'. The 'β' phase is distributed at the boundaries of the 'α' phase. Single 'V' butt joint configuration was prepared as shown in Fig. 2a to fabricate the joints using GTAW process. Square butt joint configuration was prepared as shown in Fig. 2b to fabricate the joints using EBW and LBW processes. Few trial experiments were conducted and the welded specimens were sectioned for macrographic examination to find out the complete joint penetration (CJP) and free from macro-level defect. The welding trial which produced defect free CJP was considered as the optimized welding condition (Table 2), the corresponding parameters were used to fabricate the joints. Necessary care was taken to avoid joint distortion during welding. The welding was carried out normal to the rolling direction of base metal.

The welded joints were sliced as shown in Fig. 3a, using wire-cut electric discharge machining (WEDM) to prepare fatigue and tensile test specimens. Center cracked tension (CCT) specimens were prepared (Fig. 3b) to evaluate the fatigue crack growth resistance of the welds. The slices derived from the single pass welded joints were reduced to a thickness of 5 mm by shaping and grinding processes to obtain flat and required surface roughness. Then the sharp notch was machined in the weld metal region to the required length using the WEDM process. Residual stress patterns were measured by X3000 X-ray residual stress analyzer at three different conditions: (i) as welded (AW) joints – residual stresses are measured in the fusion zone (FZ) after welding; (ii) machined and ground specimen (before machining center crack) – residual stresses are measured in the fusion zone after grinding; (iii) center cracked specimen – residual stresses are measured at the crack tip of the CCT specimens before loading into the fatigue testing

Table 1
Chemical composition of base metal (wt%).

	Al	V	Fe	O	N	C	Ti
Ti–6Al–4V	6.38	4.07	0.19	0.17	0.008	0.012	Bal.

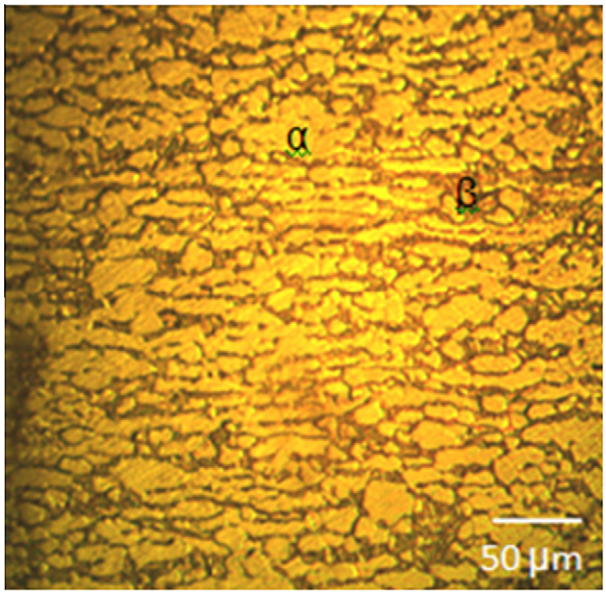

Fig. 1. Optical micrograph of base metal.

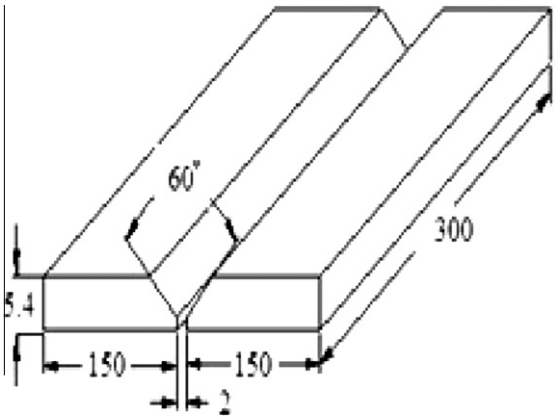

(a) Single 'V' butt joint (for GTAW)

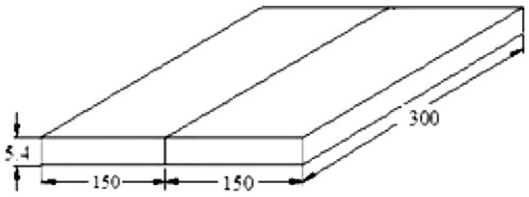

(b) Square butt joint (for LBW and EBW)

All dimensions are in 'mm'

Fig. 2. Dimensions of joint configuration.

Table 2
Welding parameters used to fabricate the joints.

Parameters	GTAW	LBW	EBW
Machine	Lincoln, USA	DC035, Slab CO_2 laser from Rofin Sinar Laser, GmbH	Techmeta, France
Polarity	AC	–	DCEN
Filler metal	ERTi-5	–	–
Electrode	Tungsten	–	Tungsten
Shielding gas	100% Argon	100% Helium	100% Argon
Current	125 A	–	50 mA
Voltage	10 V	–	50 kV
Welding speed (mm/min)	60	1500	650
Power	–	3500 W	–
Heat input (kJ/mm)	1.25	0.14	0.231

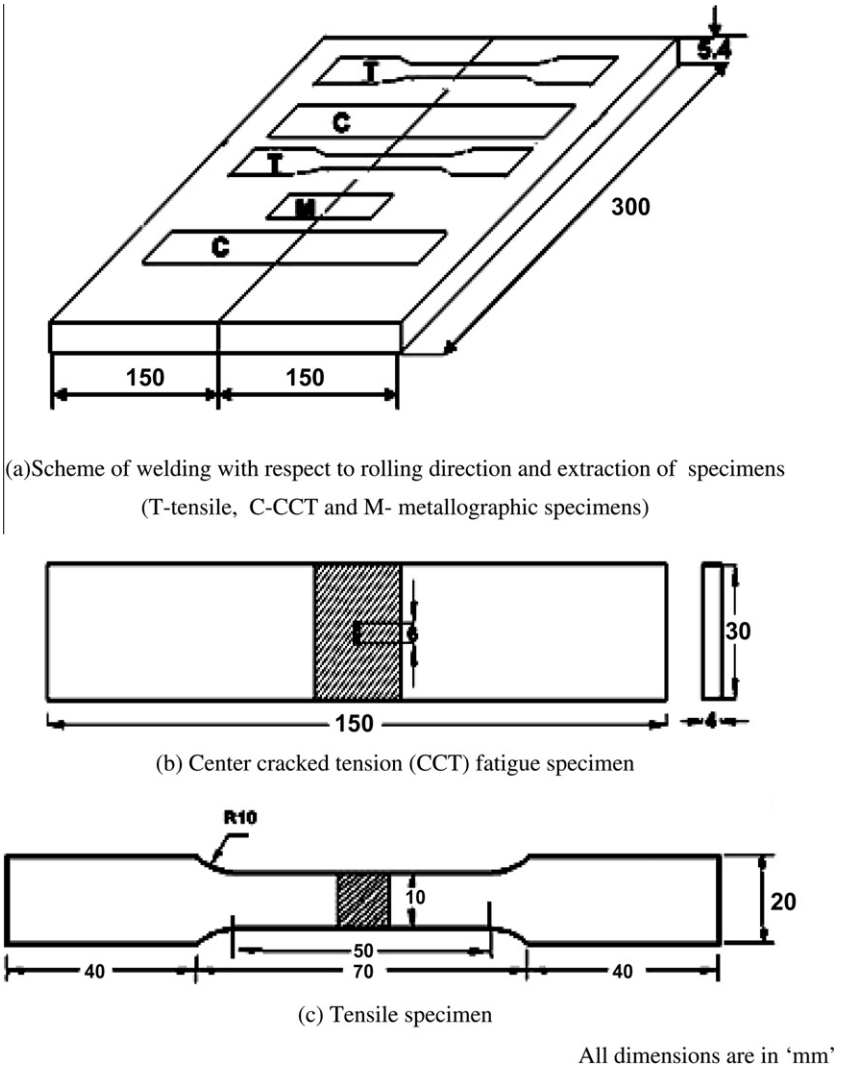

Fig. 3. Joint and specimen dimensions.

machine. Procedures prescribed by the ASTM E647-04 standard were followed for the preparation of the CCT specimens. The weld beads of the joints were machined and the effect of bead profile was eliminated in this study. The smooth tensile specimens were prepared (as shown in Fig. 3c) to evaluate yield strength, tensile strength and elongation. The tensile specimens were prepared as per the ASTM E8M-04 standard guidelines. The photographs of fabricated joints and CCT specimens are displayed in Fig. 4.

The fatigue crack growth experiment was conducted at five different stress levels (50 MPa, 75 MPa, 100 MPa, 125 MPa and 150 MPa). All the experiments were conducted under uniaxial tensile loading condition (Tension–Tension, R = stress ratio, $\sigma_{min}/\sigma_{max} = 0.1$, frequency = 10 Hz) using servo hydraulic fatigue testing machine (Make: INSTRON, UK; Model: 8801) under constant amplitude loading. Before loading, the specimen surface was polished using metallographic procedures and illuminated suitably to enable the crack growth measurement. A traveling microscope (Make: MITUTOYA; Model: 5010) attached with a web camera and video output was used to monitor the crack growth rate with an accuracy of 0.01 mm. In this investigation, the applied stress

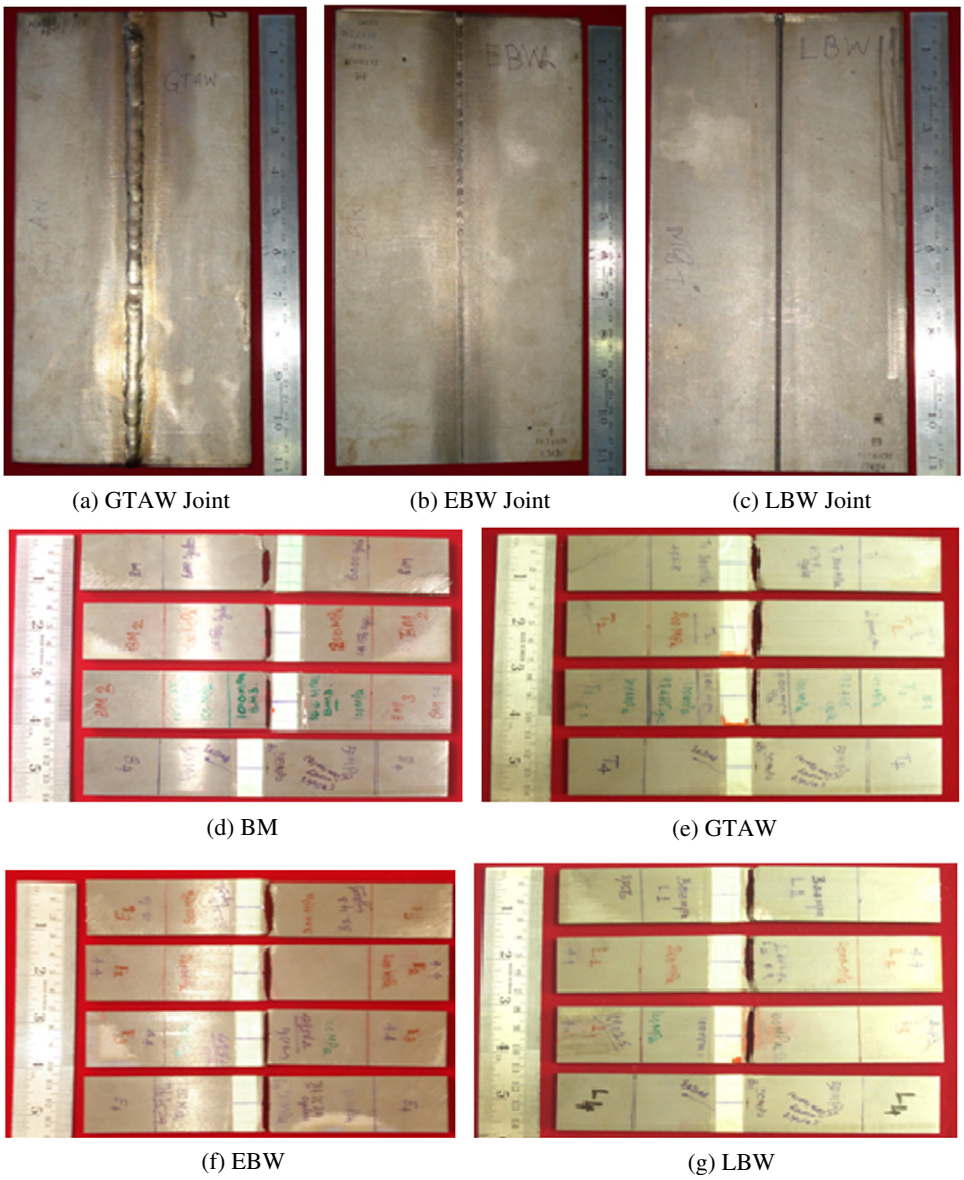

(a) GTAW Joint (b) EBW Joint (c) LBW Joint

(d) BM (e) GTAW

(f) EBW (g) LBW

Fig. 4. Photographs of joints and fatigue tested specimen.

cycle was in the tensile mode (the minimum stress was kept at $0.1P_{max}$) as the compressive mode usually closes the fatigue crack. The data points measured with an accuracy of 0.01 mm were fitted with a smooth curve as in the form of crack length vs number of cycles (a vs N).

Tensile test was carried out in 100 kN, electro-mechanical controlled Universal Testing Machine (Make: FIE-BLUE STAR, India, Model: UNITEK-94100). The specimen was loaded at the rate of 1.5 kN/min. The 0.2% offset yield strength was derived using extensometer. The percentage elongation and percentage reduction in cross sectional area were evaluated. The specimens for metallographic examination were sectioned to the required size from the weld region and polished using different grades of emery papers. Final polishing was done applying the diamond compound (1 μm particle size) in the disc polishing machine. Specimens were etched with Kroll's reagent to reveal the macro and microstructure. The micro structural analysis was done by optical microscope (Make: MEIJI, Japan; Model: ML7100). The fractured surfaces of fatigue tested specimens were analyzed using scanning electron microscope (SEM) at higher magnification to study the fracture morphology to establish the nature of the fracture.

3. Results

3.1. Fatigue crack growth results

The measured variation in crack length (2a) and the corresponding number of cycles (N) endured under the action of particular applied stress range were plotted (Fig. 5) for all the joints. The fracture mechanics based Paris Power equation [13], given below, was used to analyze the experimental results.

$$da/dN = C(\Delta K)^m \tag{1}$$

where da/dN is the crack growth rate, ΔK the stress intensity factor (SIF) range, 'C' and 'm' are constants.

The SIF value was calculated for different values of growing fatigue crack length '2a' using the following expression [14]

$$\Delta K = \phi(\Delta\sigma)\sqrt{\pi a} \tag{2}$$

However, the geometry factor 'ϕ' for the CCT specimen was calculated using the expression given below

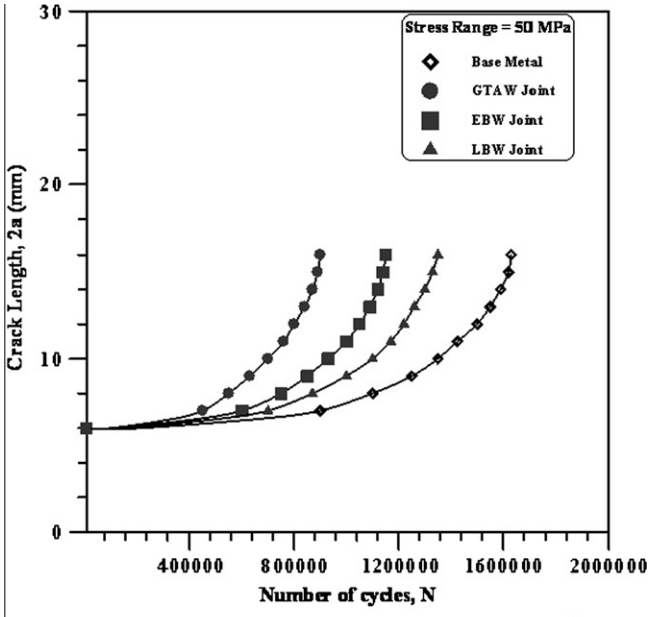

(a) Fatigue crack growth behavior at a stress range of 50 MPa

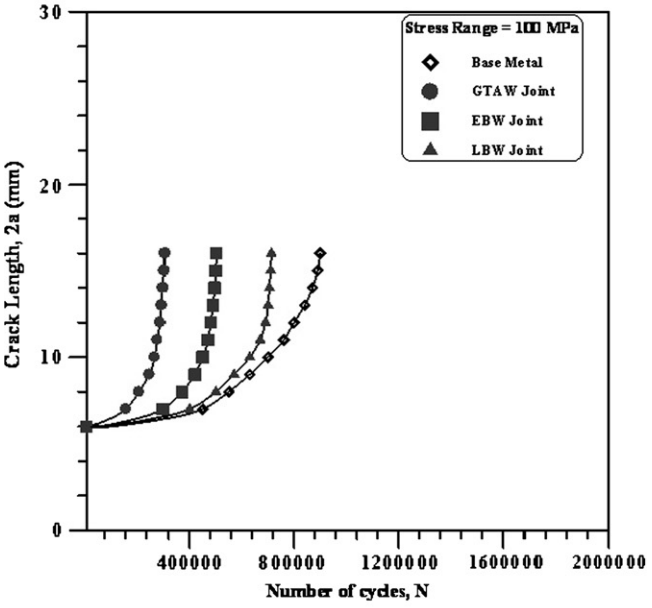

(b) Fatigue crack growth behavior at a stress range of 100 MPa

Fig. 5. Effect of welding process on fatigue crack growth behavior.

$$\phi = F(\alpha) = \sec\{(\alpha)/2\} \quad (3)$$

where $\alpha = a/W$.

The crack growth rate, da/dN for the propagation stage was calculated for steady state growth regime. The relationship between SIF range and the corresponding crack growth rate (da/dN) in terms of best fit line is shown in Fig. 6 for all joints. The data points plotted in the graph mostly correspond to the second stage of Paris sigmoidal relationship (10^{-6}–10^{-3} mm/cycle). The exponent 'm' (the slope of the line on log–log plot) and intercept 'C' of the line were determined from Fig. 6 and they are presented in Table 3.

Threshold SIF range (ΔK_{th}) and critical SIF range (ΔK_{cr}) are two important design parameters to be obtained from fatigue crack growth test. At higher values of ΔK, around 10^{-3} mm/cycle, unstable crack growth occurred and the corresponding ΔK value was

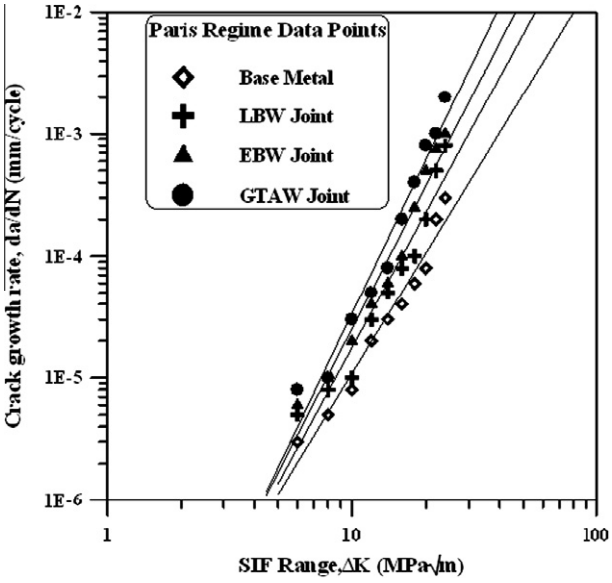

Fig. 6. Relationship between SIF range and fatigue crack rate.

Table 3
Fatigue crack growth parameters of welded joints.

Joint type	Crack growth exponent 'm'	Intercept 'C'	Threshold SIF range, ΔK_{th} (MPa $\sqrt{m}$) at 1×10^{-6} cycles	Critical SIF range, ΔK_{cr} (MPa $\sqrt{m}$) at 1×10^{-3} mm/cycles
Base metal	3.27	5.7×10^{-9}	5.0	42.5
GTAW	4.19	2.2×10^{-9}	4.0	22
EBW	3.90	3.2×10^{-9}	4.5	26
LBW	3.69	3.6×10^{-9}	4.7	30

taken as critical SIF range (ΔK_{cr}). In CCT specimen, it is very difficult to obtain the condition for non-propagating cracks due to the presence of machined notch. Hence, in the present analysis, the ΔK value at 10^{-6} mm/cycle was taken as threshold SIF (ΔK_{cr}). The values of ΔK_{cr} and ΔK_{th} for all the joints were evaluated and are presented in Table 3. The relationship between SIF range with respect to crack initiation, crack propagation and final failure is plotted and presented in Fig. 7.

3.2. Tensile test results

The transverse tensile properties such as yield strength, tensile strength and percentage elongation of Ti–6Al–4V alloy joints were evaluated. In each condition, three specimens were tested, and the average of three results is presented in Table 4. The yield strength and tensile strength of unwelded base metal are 970 MPa and 1010 MPa, respectively. But the respective yield strength and tensile strength of GTAW joint are 890 MPa and 940 MPa. This indicates 7% reduction in strength values due to GTAW process. The yield strength and tensile strength of LBW joint are 960 MPa and 1000 MPa, respectively which are 1% lower compared to base metal. However, the yield strength and tensile strength of EBW joint are 950 MPa and 985 MPa, respectively. Of the three welded joints, the joint fabricated by LBW process exhibited higher strength values, and the difference is 6% higher compared to GTAW joints and 2% higher compared to EBW joints.

Elongation of unwelded base metal is 12.7% but the elongation of GTAW joint is 10.15%. This suggests 20% reduction in ductility

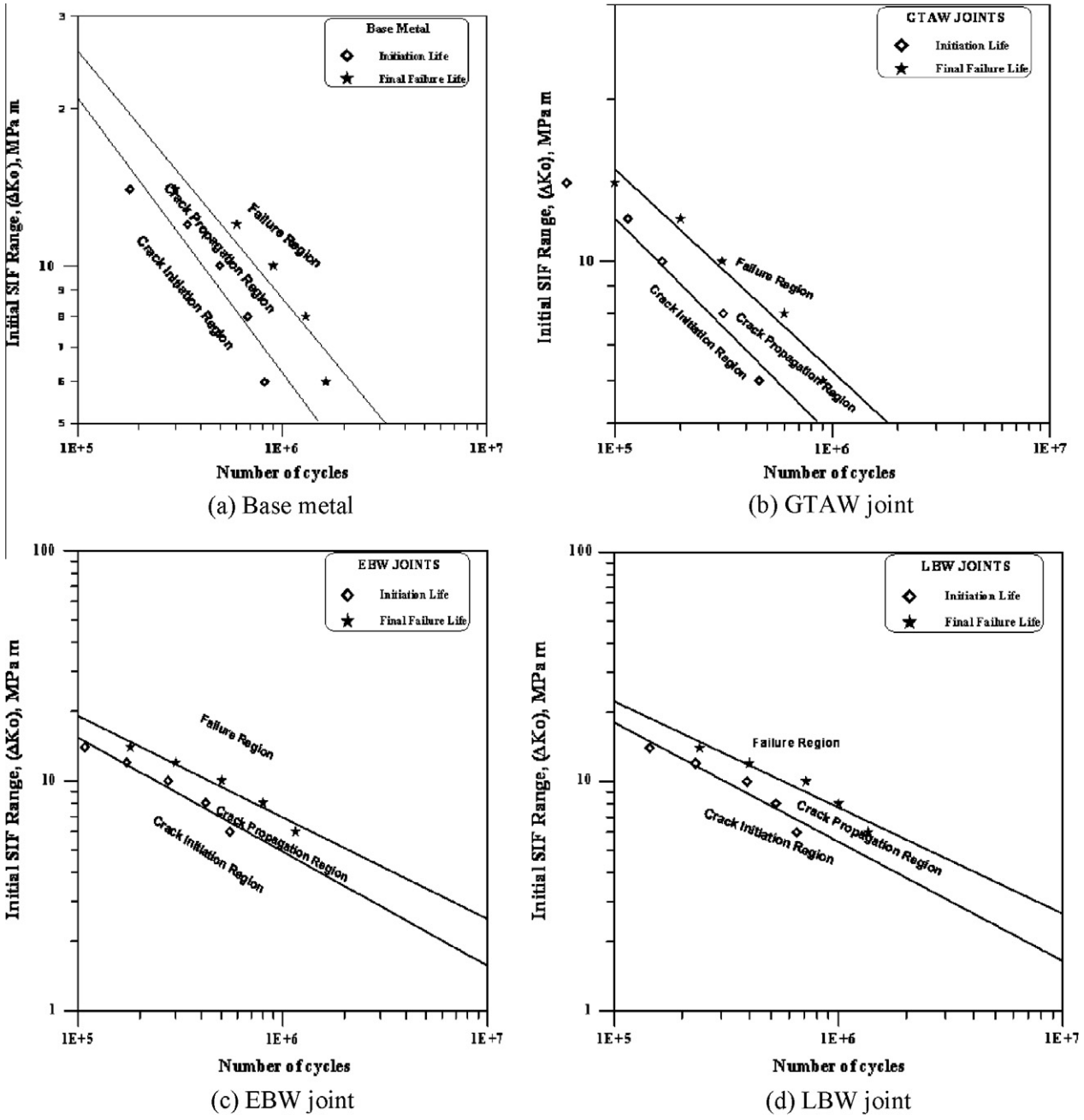

Fig. 7. Crack growth behavior of base metal and welded joints.

Table 4
Transverse tensile properties of base metal and welded joints.

	0.2% offset yield strength (MPa)	Ultimate tensile strength (MPa)	Elongation in 50 mm gauge length (%)	Weld metal hardness in HV at 0.05 kg
Base metal	970	1010	12.7	372
GTAW	890	940	10.15	390
LBW	960	1000	15.00	463
EBW	950	985	7.70	488

due to GTAW process. Similarly, the elongation of LBW joints is 15%, which is 18.1% higher compared to the base metal. However, the elongation of EBW joint is 7.7%. Of the three welded joints, the joint fabricated by LBW process showed higher ductility values, and the difference is 48% higher compared to GTAW joint and 95% higher compared to EBW joint.

3.3. Residual stress

Table 5 shows the measured residual stress values, from which one can identify the residual stress value arise in welded joints as a consequence of incompatible thermal strains caused by heating and cooling cycles. Out of the three welding processes used in this investigation, the heat input involved in GTA welding process is relatively higher compared to EBW and LBW processes (refer Table 2). Hence the magnitude of tensile residual stress in gas tungsten arc (GTA) welded joints are higher compared to EBW and LBW joints and this is also evident from the measured residual

Table 5
Residual stress measurement results of welded joints.

Joint type	Magnitude of residual stress (MPa)		
	As welded joint (fusion zone)	Machined and ground specimen (fusion zone)	Center cracked specimen (tip of the crack)
GTAW	+120	+20	+4
EBW	+80	−20	0
LBW	+60	−40	−2

stress values presented in Table 5. In the machined and ground specimens, the measured residual stress values are lower compared to as welded joints and this is mainly due to the reason that after welding the joints were sliced, machined and ground to obtain the required dimensions of CCT specimen. The magnitude of original tensile residual stresses caused by welding operation are reduced due to the compressive load acted on the specimen during grinding operation. The remaining residual stresses are also relieved during machining a sharp notch at the weld center using wire-cut electric discharge machining process. This is evident from the measured residual stress values at the crack tip. Further, the residual stresses are usually relieved during fatigue cycling due to high strains/stress concentrations around the crack front. From the above results it is inferred that the magnitude of residual stress nearer to the crack tip in all the three joints is almost similar. Though the residual stresses will have significant influence on the fatigue behavior of welded joints, in the present investigation, it is found that the residual stresses do not have significant influence on the fatigue crack growth behaviour of welded titanium alloy joints due to specimen configuration.

3.4. Microstructure

Optical micrographs of weld metal region of the joints are presented in Fig. 8. Fusion zone microstructure of GTAW joint (Fig. 8a) containing the coarse serrate and acicular α structures of grain boundary α, massive α, and Widmanstätten α + β [15]. The weld fusion zone in titanium alloys is characterized by coarse, columnar prior-beta grains that originate during weld solidification. The size and morphology of these grains depend on the nature of the heat flow that occurs during weld solidification. The fusion-zone beta grain size depends primarily on the weld energy input, with a higher energy input promoting a larger grain size. The reason for the grain coarsening of the GTAW joint can be justified to the heat input involved in this process. The heat input supplied here was 1.25 kJ/mm (Table 3) which was higher compared to LBW and EBW processes. The higher heat input led to longer cooling time resulting the grain growth and resulted in coarse grained structure of massive α, and Widmanstätten α + β. Three-dimensional or

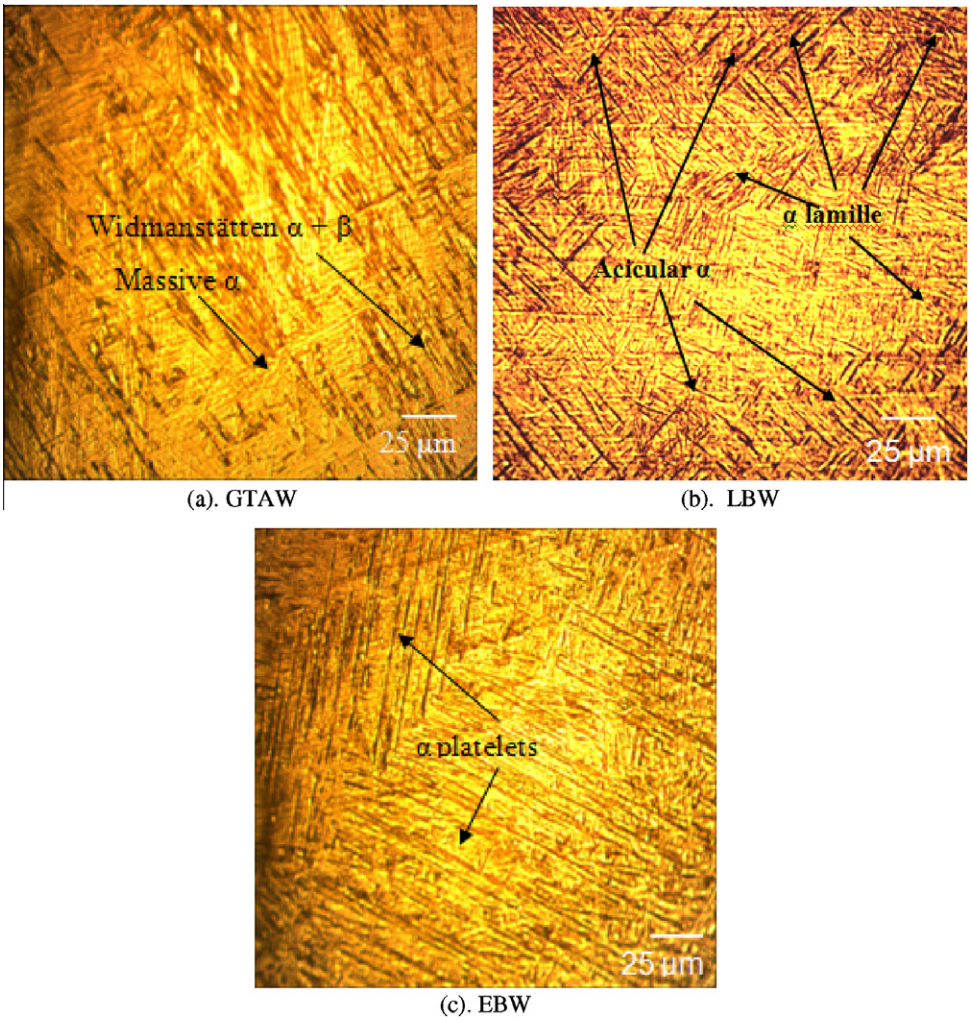

Fig. 8. Optical micrograph of weld metals.

mixed two-dimensional/three dimensional heat-flow conditions, such as those present in single-pass and multi pass gas tungsten arc weldments, promoted the formation of more complex, multidirectional beta grain morphologies. The lower cooling rates associated with GTAW (10–100 °C/s), resulted in a coarse structure of Widmanstätten alpha plus retained beta, or a mixture of this structure and alpha-prime [16].

Fig. 8b shows the EBW joint microstructure and it contains the serrate and regular plate-shaped α structures. The microstructure of LBW joint shows fine lamellar and acicular 'α' structure (Fig. 8c). The heat input associated with this process is 0.14 kJ/mm was the lowest of the three processes. Lowest heat input led to faster cooling rate (100–10,000 °C/s) and finer microstructure of α lamellae. The formation of the acicular grains is due to the fast cooling rate associated with LBW process and the plate-like α is due to the slow cooling rate of EBW process [1]. The slower cooling rate in EBW process may be contributed due to welding in vacuum chamber. The heat input (0.231 kJ/mm) in EBW process was intermediate between GTAW and LBW processes. Comparatively higher heat input and slower cooling rate than LBW process resulted 'α' platelets instead of lamellae because the lamellae are allowed to grow up to some extent.

3.5. SEM fractographs

The fatigue fracture surface appearance corresponding to crack initiation, crack propagation and the final failure regions of base metal, GTAW, EBW and LBW joints, as observed under the SEM is displayed in Figs. 9–11. Here, the fatigue crack initiation region (FCI) is corresponding to 1 mm from the tip of the machined notch; fatigue crack propagation (FCP) region is referred to 1–6 mm; final failure (FF) region is referred to 6 mm away from the crack initiation region. For fracture surface analysis, the specimens tested at 50 MPa applied stress range level were taken from all the joints to make comparative analysis.

Fig. 9 shows the fracture surface morphology of fatigue crack initiation (FCI) region. In all the joints, the crack initiation sites are clearly visible and it can be observed from the fractographs that the fatigue cracks have initiated from multiple crack initiation sites. Base metal fractograph (Fig. 9a) shows the presences of many small voids, which bear little resemblance to conventional dimples, are visible among the small facets. A typical Stage I fatigue fracture is observed in GTAW joint (Fig. 9b). Stage I fatigue fracture surface is faceted, often resemble cleavage, and does not exhibit fatigue striations. Stage I fatigue is normally observed on high-cycle low-stress fractures and is frequently absent in low cycle high-stress fatigue [17]. The micro-level striations are observed in the 'β' grains since the 'α' grains are probable crack initiation sites (Fig. 9c), in the EBW joint. Tearing topography surface (TTS), ductile rupture (DR) and cleavage mode of fracture are observed in LBW joint (Fig. 9d). TTS are generally characterized by relatively smooth, often flat, areas or facets that usually contain thin tear ridges (Fig. 9a–d). River pattern of cleavage sites are also visible at the bottom right corner in the fractograph (Fig. 9d). Large numbers of crack initiation sites are seen in GTAW joints, comparatively lesser nucleation site only visible in base metal whereas moderate numbers of crack initiation sites are observed in EBW and LBW welds.

Fig. 10 reveals the fracture surface appearance of fatigue crack propagation (FCP) region (where steady state crack growth occurred). Invariably in all the joints, the fracture surface shows the crack arrest marks known as fatigue striations, which are the visual record of the position of the fatigue crack front during crack propagation through the material. The base metal fractograph

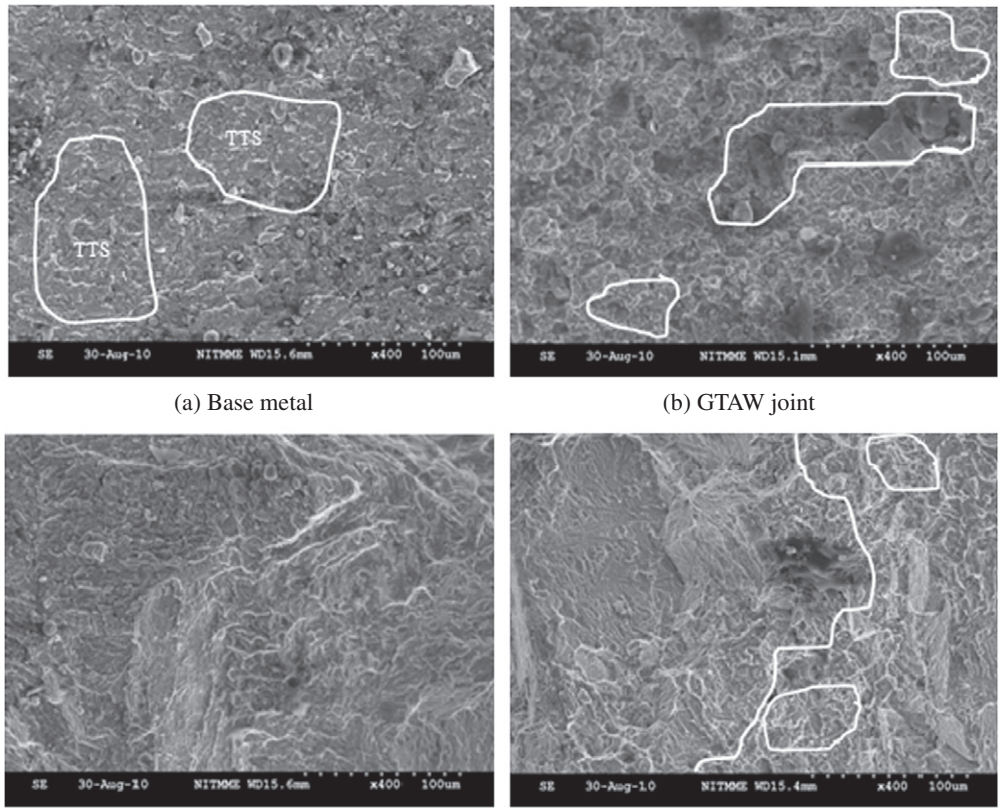

(a) Base metal (b) GTAW joint

(c) EBW joint (d) LBW joint

Fig. 9. Fractographs of FCI region.

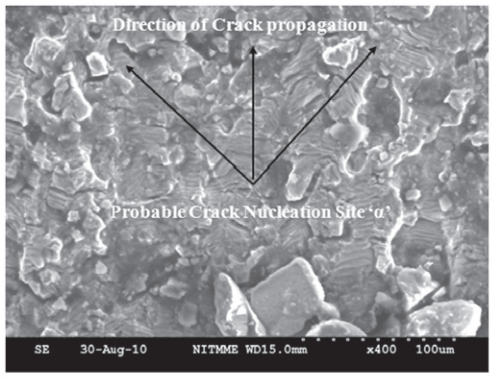

(a) Base metal

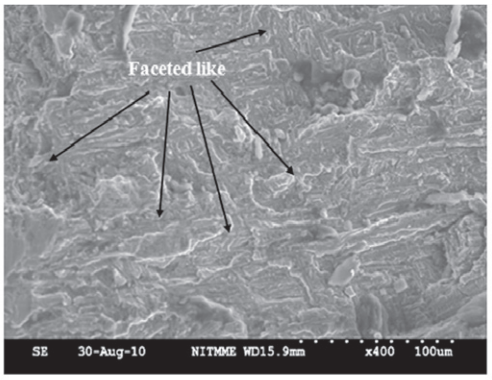

(b) GTAW joint

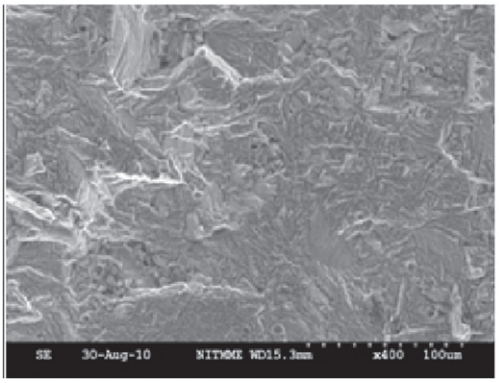

(c) EBW joint

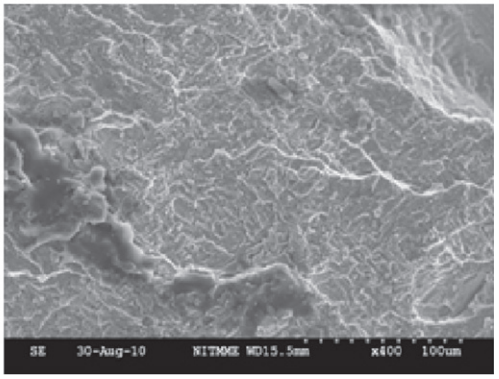

(d) LBW joint

Fig. 10. Fractographs of FCP region.

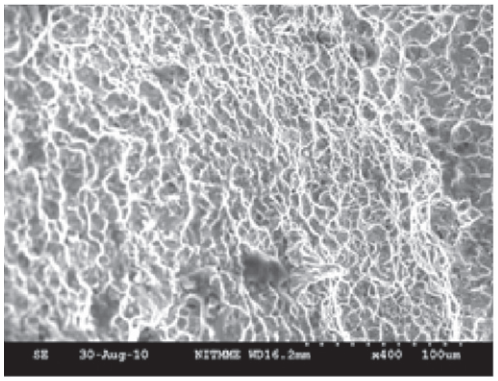

(a) Base metal

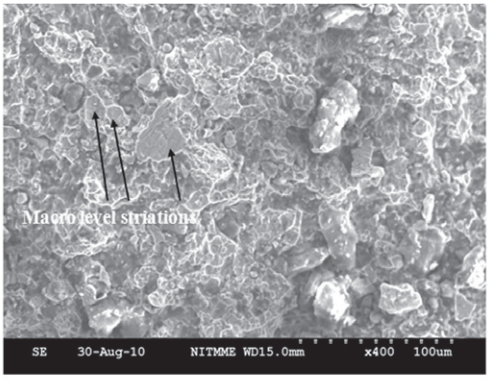

(b) GTAW joint

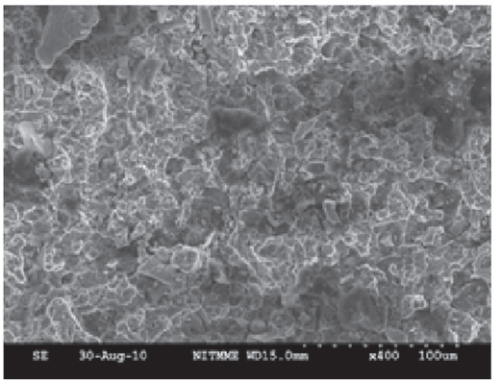

(c) EBW joint

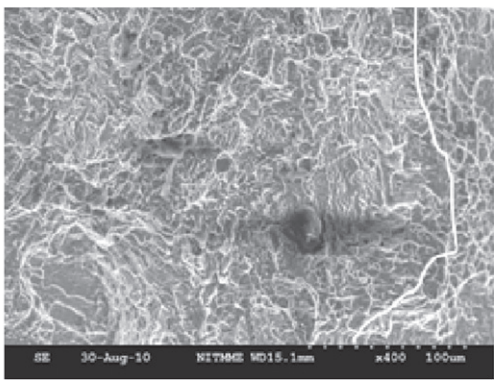

(d) LBW joint

Fig. 11. Fractographs of FF region.

shows the presence of striations in the facets itself (Fig. 10a). This can be adjudged by the characteristic feature of the fatigue striations: The striations are parallel and right angles to the local direction of crack propagation. The crack initiation sites can be identified by drawing an imaginary radius perpendicular to striation direction and centered at the origin. The direction of crack propagation is indicated by arrow mark. GTAW weld fractograph (Fig. 10b) clearly reveals the presence of transgranular facets with some secondary cracking. In EBW joint fractograph (Fig. 10c) the change from transgranular facets to dimples like fracture surface is clearly visible. LBW joint fractograph presented in Fig. 10d reveals the fine intergranular fracture surface appearance in addition with few micro cracks and isolated dimples. From the FCP region fractography, it is understood that the spacing between striations is wider in GTAW joint, closer in base metal and intermediate in EBW and LBW joints.

Fig. 11 exhibits the fracture surface appearance of final failure region (FF) region (where unstable crack growth occurred) of all the joints. From the fractographs it is observed that the tear dimples are elongated along the loading direction and this is mainly because of the limit load condition at the time of final fracture. Even though unstable crack growth occurred in the final failure region, the final fracture took place in the ductile mode and it is evident from the presence of dimples. The mode of failure for the final failure (FF) region of base metal and the welds are a combination of ductile with microvoid coalescence called DR and TTS. The fractograph of base metal presented in Fig. 11a reveals the structure of ductile mode failure with dimples of fine size. The macro-level striations are observed in the 'β' grains since the 'α' grains are probable crack initiation sites (Fig. 11b) in the GTAW joint. EBW fractograph (Fig. 11c) shows the presences of many small voids, which bear little resemblance to conventional dimples, are visible among the small facets. In EBW joint, facets are the dominant failure pattern, but in LBW joint cleavage facets and dimples are clearly visible. To summarize, the final fracture surface of base metal contains only dimples; higher amount of facets and less area of dimples are observed in GTAW joint; both facets and dimples are seen in EBW and LBW joints. In EBW joint the dimples are presented in isolated locations while in LBW joint the dimples are continuous in a particular area. This suggests that the resistance offered by LBW joint against the growing fatigue crack, even in the unstable crack growth region, is much better than other joints.

4. Discussion

From the fatigue crack growth test results (Table 3), it is understood that the LBW joint is exhibiting superior fatigue crack growth resistance compared to GTAW and EBW joints. The fatigue crack growth exponent was obtained from the slope of the curve drawn between da/dN and SIF range. If this exponent is lower, then slope of the curve is lower and the resistance offered by the material to the growing fatigue crack is higher and hence the fatigue life is longer. If this exponent is larger, then slope of the curve is higher and the resistance offered by the material to the growing fatigue crack is lower and hence the fatigue life is shorter. The reasons for the better fatigue crack growth resistance of the LBW joint are: (i) superior tensile properties of the welded joint and (ii) preferable microstructure in the weld region.

4.1. Superior mechanical properties

Transverse tensile properties of the base metal and welded joints presented in Table 4 indicate that the LBW joint is exhibiting higher yield strength compared to GTAW and EBW joints. During tensile test, all the specimens invariably failed in the weld metal. This indicates that the weld metal is comparatively weaker than other regions and hence the joint strength is controlled by the weld metal strength. The mechanical properties (yield strength, tensile strength and elongation) of LBW joint are superior compared to other joints (see Table 4). Higher yield strength of the LBW joint is greatly used to enhance the endurance limit of the LBW joint and hence the fatigue crack initiation is delayed. Larger elongation (higher ductility) of the LBW joint also imparts greater resistance to fatigue crack propagation and hence fatigue crack growth rate is comparatively slower. The combined effect of higher yield strength and higher ductility of the LBW joint offers enhanced resistance to crack initiation and crack propagation and hence the fatigue performance of the LBW joint is superior compared to GTAW and EBW joints.

In lower strength weld metal (as in the case of GTAW), the deformation and the yielding are mainly concentrated in the weld metal zone and the extension of the plastic zone is limited within the weld metal. Eripret and Hornet [18] stated that as soon as the plastic zone reaches the fusion line, plasticity keeps on developing along the interface between the parent material and the weld metal. The triaxial state of stress is high in the weld metal and the relaxation of this stress is poor. The crack driving force needed for crack extension is small. Hence, the fracture toughness of the lower strength weld metal is not high. On the other hand, if strength of the weld metal is more or less equal to the base metal, as in the case of LBW joint, the plastic zone can easily extend into the parent material because the deformation and yielding occur in both weld metal and the base metal. The stress relaxation can easily take place in the crack tip region. Ghosh et al., [19] opined that more crack driving force is needed for crack extension and the fracture resistance of the higher strength weld metal is greater than the lower strength weld metal. This is also one of the reasons for superior fatigue crack growth resistance of the LBW joint.

4.2. Preferable microstructure

In CCT specimen, the notch is machined in the weld metal (weld center line) region of joints by WEDM process to evaluate the crack growth behaviour of the weld metal under fatigue loading. The fatigue crack initiates from the tip of the machined notch and it grows in the weld region until final failure takes place and hence the weld metal microstructure surely has an influence on fatigue performance of the joints. The fatigue properties of metals are quite structure sensitive. The microstructure of the weld metal is influenced by the heat input of the welding processes. Of the three welding processes used in this investigation to fabricate the joints, the GTAW process recorded higher heat input compared to the LBW and EBW processes (Table 2). Generally, higher heat input will lead to slower cooling rate and slow cooling rate will result in coarse microstructure. The lower strength of GTAW joint may be attributed by the presence of coarse serrate structures of grain boundary α, massive α, and Widmanstätten α + β. The moderate yield strength of EBW joint could be contributed to the weld metal microstructure containing of fine serrate and regular plate-shaped 'α' microstructures. Though the plate shaped microstructures is comparatively finer than GTAW joint, it is coarser than the fine lamellar microstructure resulted in LBW joint. Thus EBW joint shows intermediate yield strength between GTAW and LBW joints. Higher yield strength exhibited by the LBW joint might be due to the presence of fine lamellar and acicular morphology in the weld metal. In this joint, the presence of martensitic structure is also observed. It was reported that cooling rates higher than 410 °C/s are usually required for Ti–6Al–4V alloy to attain a completely martensitic structure [20]. The high self- quenched rate associated with the laser beam welding process certainly promotes the

diffusion less transformation of the 'β' phase into martensitic microstructure.

The microstructure of the weld metal region will have greater influence on the fatigue performance of the joint than weld bead geometry, joint design etc. Microstructure invariably affects the fatigue strength by increasing the propensity for crack nucleation and its early growth, causing the ultimate failure of the joint. In addition to α grain size, degree of age hardening, and oxygen content, the fatigue properties of two-phase α + β alloys are strongly influenced by the morphology and arrangements of the two-phases 'α' and 'β'. Equiaxed microstructure is presented in base metal, whereas lamellar, acicular and bimodal microstructures (primary α in a lamellar matrix) are seen in LBW, EBW and GTAW joints [15]. In lamellar microstructures (Fig. 8b and c), fatigue cracks initiate at slip bands within 'α' lamellae or at 'α' along prior 'β' grain boundaries [21]. Since the resistance to dislocation motion as well as fatigue crack initiation depends on the 'α' lamellae width, there is a direct correlation between fatigue strength and yield stress. For equiaxed structures, fatigue cracks nucleate along slip bands within 'α' grain (Fig. 1). Thus, fatigue strength correlates directly with the grain size dependent yield stress. In duplex structures, fatigue cracks can either initiate in the lamellar matrix, at the interface between the lamellar matrix and the primary 'α' phase, or within the primary α phase (Fig. 8a). The precise crack initiation site depends on the cooling rate [22], and the volume fraction and size of the primary 'α' phase [20,21]. For a lamellar microstructure, lamellar width should be considered instead of grain size.

A reduction of prior β grain size in lamellar microstructures and a reduction of the primary 'α' volume fraction in duplex structures increase both low cycle fatigue life as well as fatigue strength [23,24]. Simultaneously, this structural modification increases the resistance to crack growth. Therefore, the fine grained lamellar microstructure shows superior resistance to crack growth behaviour over the coarse grained lamellar structure, while for duplex structures the lower primary α volume fraction is superior to the higher one. The latter can probably be explained by the (near) absence or lower presence of agglomerates of primary α grains and simultaneously reduced primary α volume fraction. This primary α cluster can act as large single grains, which are easy for micro cracks to propagate through. Thus the joints consisting coarse lamellar (EBW), bimodal (GTAW) yields lower fatigue crack growth resistance than the joint having fine lamellar microstructure (LBW). The presence of fine lamellar microstructure in the weld metal enhanced the yield strength and ductility of the LBW joint. Fine lamellar in addition with acicular morphology (inter locking nature of multi directionally oriented grains) play an important role for the resultant tensile and ductility of the LBW joint. It is well known that a structure containing a large percentage of lamellar 'α' offers greater resistance to crack growth than equiaxed structures. This can be usually ascribed to the fact that crack path deviations and bifurcations can occur more easily in plate like structures [25]. The improvement in the yield strength and ductility are the reasons for higher fatigue crack growth resistance of LBW joint.

5. Conclusions

In this investigation, the fatigue crack growth parameters of GTAW, LBW and EBW joints of Ti–6Al–4V titanium alloy were evaluated. The important conclusions from this investigation are:

(i) Fatigue crack growth resistance of Ti–6Al–4V alloy is greatly reduced by the welding processes. However, the joint fabricated by LBW process exhibited higher fatigue crack growth resistance ($m = 3.69$) than EBW ($m = 3.9$) and GTAW ($m = 4.19$) joints.

(ii) Though the threshold SIF range of Ti–6Al–4V alloy is not influenced significantly by the welding processes (varies between 4 and 5 MPa $\sqrt{m}$), the critical SIF range is appreciably influenced by the welding processes (varies between 20 and 40 MPa $\sqrt{m}$).

(iii) Higher yield strength and higher ductility due to the presence of very fine lamellar shaped 'α' microstructure in the weld metal are the main reasons for the superior fatigue performance of the LBW joints compared to GTAW and EBW joints. Lower heat input and faster cooling rate associated with LBW process is mainly responsible for the formation of very fine lamellar 'α' in weld metal

Acknowledgements

The authors wish to record their sincere thanks to the Combat Vehicles Research and Development Establishment (CVRDE), Avadi, Chennai, Government of India for providing financial support to carry out this investigation through a Contract Acquisition for Research Services Project, No. CVRDE/MMG/09-10/0043/CARS. The authors also register their sincere thanks to Defense Research & Development Laboratory (DRDL), Hyderabad for effective fabrication of the joints. The authors express their sincere thanks to M. Balakrishnan, Project Associate, CEMAJOR, Annamalai University for his useful contribution to carryout this investigation.

References

[1] Yunlian Qi, Ju Deng, Quan Hong, Liying Zeng. Electron beam welding, laser beam welding and gas tungsten arc welding of titanium sheet. Mater Sci Eng 2000;A280:177–81.
[2] Saresh N, Gopalakrishna Pillai M, Mathew Jose. Investigations into the effects of electron beam welding on thick Ti–6Al–4V titanium alloy. J Mater Process Technol 2007;192–193:83–8.
[3] Balasubramanian M, Jayabalan V, Balasubramanian V. A mathematical model to predict impact toughness of pulsed-current gas tungsten arc-welded titanium alloy. Int J Adv Manuf Technol 2008;35:852–8.
[4] Noolua NJ, Kerra HW, Zhoua Y, Xieb J. Laser weldability of Pt and Ti alloys. Mater Sci Eng A 2005;397:8–15.
[5] Balasubramanian M, Jayabalan V, Balasubramanian V. Prediction and optimization of pulsed current gas tungsten arc welding process parameters to obtain sound weld pool geometry in titanium alloy using lexicographic method. ASM Int, JMEPEG 2009;18:871–7.
[6] Keshava murthy K, Sundaresan S. Fatigue crack growth behavior in a welded α–β Ti–Al–Mn alloy in relation to the microstructural features. Mater Sci Eng 1997;A222:201–11.
[7] Saxena Vikas Kumar, Radhakrishnan VM. Effect of phase morphology on fatigue crack growth behavior of a–b titanium alloy—a crack closure rationale. Metall Mater Trans A 1998;29A:245–61.
[8] Sinha V, Mercer C, Soboyejo WO. An investigation of short and long fatigue crack growth behavior of Ti–6Al–4V. Mater Sci Eng 2000;A287:30–42.
[9] Boyce BL, Ritchie RO. Effect of load ratio and maximum stress intensity on the fatigue threshold in Ti–6Al–4V. Eng Fract Mech 2001;68:129–47.
[10] Tsay LW, Shan YP, Chao Y-H, Shu WY. The influence of porosity on the fatigue crack growth behavior of Ti–6Al–4V laser welds. J Mater Sci 2006;41:7498–505.
[11] Ding YS, Tsay LW, Chen C. The effects of hydrogen on fatigue crack growth behaviour of Ti–6Al–4V and Ti–4.5Al–3V–2Mo–2Fe alloys. Corros Sci 2009;51(6):1413–9.
[12] Wang Xuedong, Shi Qingyu, Wang Xin, Zhang Zenglei. The influences of precrack orientations in welded joint of Ti–6Al–4V on fatigue crack growth. Mater Sci Eng 2010;A527(4–5):1008–15.
[13] Paris PC, Erdogan F. Basic engineering. Trans ASTM J 1963:528–34.
[14] Hellan K. Introduction to fracture mechanics. 2nd ed. New York: McGraw Hill Book Company; 1984. p. 172–3.
[15] ASM Hand Book, vol. 9 – metallography & microstructures. p. 968–1015.
[16] ASM Hand Book, vol. 6 – welding, brazing and soldering. p. 740–54, 1289–30.
[17] ASM Hand Book, vol. 12 – fractography. p. 768–93.
[18] Eripret C, Hornet P. Prediction of overmatching effects on the fracture of stainless steel cracked welds. In: Schwalbe KH, Kocak M, editors. Mismatching of welds, ESIS 17. London: Mechanical Engineering Publications; 1994. p. 685–708.
[19] Potluri NB, Ghosh PK, Gupta PC, Reddy YS. Studies on weld metal characteristics and their influences on tensile and fatigue properties of pulsed current GMA welded Al–Zn–Mg alloy. Weld Res Suppl 1996;1:62s–70s.

[20] Ahmed T, Rack HJ. Phase transformation during cooling in α+β titanium alloys. Mater Sci Eng 1998;A243:206–11.
[21] Mohandas T, Banerjee D, Kutumba Rao VV. Fusion zone microstructure and porosity in electron beam welds of an a + b titanium alloy. Metal Trans 1998;30A:789–98.
[22] Thompson AW, Chesnutt JC. Metall Trans A 1979;10A:1193.
[23] Magudeeswaran G, Balasubramanian V, Balasubramanian TS, Madhusudhan Reddy G. Effect of welding consumables on tensile impact properties of shielded metal arc welded high strength, quenched and tempered steel joints. Sci Technol Weld Join 2008;13:97–105.
[24] Berg A, Kiese J, Wagner L. In: Lee EW, Jata KV, Kim NJ, Frazier WE, editors. Light-weight alloys for aerospace applications III. TMS; 1995. p. 407.
[25] Leyens C, Peters M, editors. Titanium and titanium alloys (fundamentals and applications). Weinheim: Wiley-VCH Verlag GmbH & Co. KGaA; 2003. p. 153–86 [ISBN: 3-527-30534-3].